AIAA SciTech Forum
January 3-7, 2022, San Diego, CA & Virtual
AIAA SCITECH 2022 Forum

10.2514/6.2022-1731

Check for updates

Assembly Integration and Test of the Lunar Flashlight Propulsion System

Celeste R. Smith[1], Lacey M. Littleton[2], E. Glenn Lightsey[3]
Georgia Institute of Technology, Atlanta, Georgia 30313

Daniel Cavender[4]
Marshall Space Flight Center, Huntsville, Alabama, 35808

Downloaded by GEORGIA INST OF TECHNOLOGY on February 26, 2022 | http://arc.aiaa.org | DOI: 10.2514/6.2022-1731

The Lunar Flashlight Propulsion System (LFPS) was created to perform a Lunar Orbital Insertion maneuver for the Lunar Flashlight spacecraft so it can conduct its search for water in the lunar South Pole. The focus of this paper is on the late-stage design, integration, and test of the LFPS. The structure of the LFPS is 3D printed and further 3D printing was utilized to assist in the assembly process. The design will be reused to build a second unit and its heritage is already being leveraged on other early concept propulsion systems.

I. Introduction

Lunar Flashlight (LF) is a 6U CubeSat mission selected by NASA's Advanced Exploration Systems (AES) to search for ice in permanently shadowed craters near the lunar South Pole. The mission is led by a team from the Jet Propulsion Laboratory (JPL) with Marshall Space Flight Center (MSFC) providing the required propulsion system. Lunar Flashlight was originally planned for launch aboard Artemis-1 as a secondary payload which would be deployed into a lunar flyby trajectory. Due to delays during development, the LF spacecraft was de-manifested from Artemis-1 and is now manifested for launch on a new vehicle in 2022. After deployment from the upper stage, the LF spacecraft will perform a lunar orbital insertion maneuver which will result in the desired polar orbit. The Lunar Flashlight Propulsion System (LFPS) was developed in a partnership by NASA's Marshall Space Flight Center (MSFC) and the Glenn Lightsey Research Group (GLRG) at the Georgia Institute of Technology (GT). In less than 2 years, this team designed, built, and acceptance tested a novel, 'green' chemical propulsion system. This paper covers the assembly and testing of the LFPS flight unit, which was performed from Fall 2020 to Spring 2021. That unit was delivered to the Lunar Flashlight Project at NASA's Jet Propulsion Laboratory (JPL) in May 2021 and has since completed integration and testing with the LF spacecraft. The LF spacecraft will be sent to MSFC for fueling in early 2022.

[1] Graduate Research Assistant, Department of Aerospace Engineering, celestesmith@gatech.edu
[2] Graduate Research Assistant, Department of Aerospace Engineering, llittleton3@gatech.edu
[3] Professor, Department of Aerospace Engineering, glenn.lightsey@gatech.edu
[4] Deputy Chief Technologist, daniel.p.cavender@nasa.gov

Copyright © 2022 by Georgia Institute of Technology. Published by the American Institute of Aeronautics and Astronautics, Inc., with permission.

Additionally, the team is building a second LFPS unit as a low-cost propulsion system for use on a future NASA mission.

The LFPS uses the ASCENT (Advanced Spacecraft Energetic Non-Toxic) propellant with a pump-fed design which is low pressure at launch. This pump-fed approach significantly reduces the system's assessed hazard risk while meeting the impulse requirements for the mission. This mission also provides further demonstration of small satellite propulsion systems using the ASCENT propellant. This paper will share insights about the flight system's assembly, integration, acceptance, and qualification activities during this fast-paced project.

The LFPS delivers more than 3300 N-s of total impulse during the LF mission while fitting within a 2.5U CubeSat volume (25 cm x 10 cm x 10 cm). This small volume was enabled by additive manufacturing techniques which allowed fluid passages to be built directly into the structure [1].

Downloaded by GEORGIA INST OF TECHNOLOGY on February 26, 2022 | http://arc.aiaa.org | DOI: 10.2514/6.2022-1731

II. System Overview

The LFPS consists of two main subassemblies – the propellent tank and manifold. The propellant tank subassembly includes a two-piece welded propellant tank structure, a fill/drain valve, propellant isolation valve, a propellant management device (PMD), a propellant filter, a pressure sensor, two thin, flexible Kapton heaters, and three thin, flexible thermocouples to monitor heater and tank temperature.

The manifold subassembly is a 3D printed titanium structure with integrated flow passages, four thruster valves, an electric propellant pump with a brushless DC motor, a propellant recirculation block, a pressure sensor, the controller, and four 100 mN thrusters. The pump is mounted in the middle of the manifold. The controller boards are mounted to the manifold, straddling the pump. To protect the electronics and pump, a 2-mm thick titanium 6Al-4V electrical enclosure is mounted over the top (known as the "muffin tin"). This enclosure provides external and ancillary component mounting and radiation protection.

Downloaded by GEORGIA INST OF TECHNOLOGY on February 26, 2022 | http://arc.aiaa.org | DOI: 10.2514/6.2022-1731

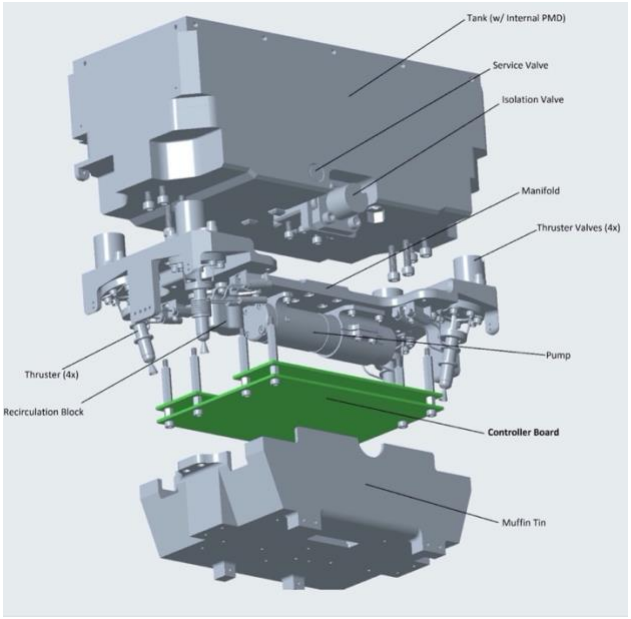

Figure 1. The LFPS expanded view

III. System Integration

A non-serial assembly flow was designed into the LFPS from the beginning and leveraged to the greatest extent possible. This approach provided the team with great flexibility in responding to technical and programmatic challenges when they arose. But, as the assembly progressed, the workflow became more serialized as the design constraints limited that flexibility.

A. Assembly, Integration, and Test Procedures (AITPs)

The LFPS Product Breakdown Structure (PBS), shown in Figure 2, shows how the Project "broke down" to the LFPS components and sub-assemblies into one of several Assembly, Integration, and Test Procedures (AITPs) that detailed how the system build-up would be executed. The legend detailed what type of 'artifact' would control that item, such as machine or process drawing, interface control document (ICD), etc. It also detailed who was responsible for producing that product. The PBS was used as a 'workflow' representation and roadmap.

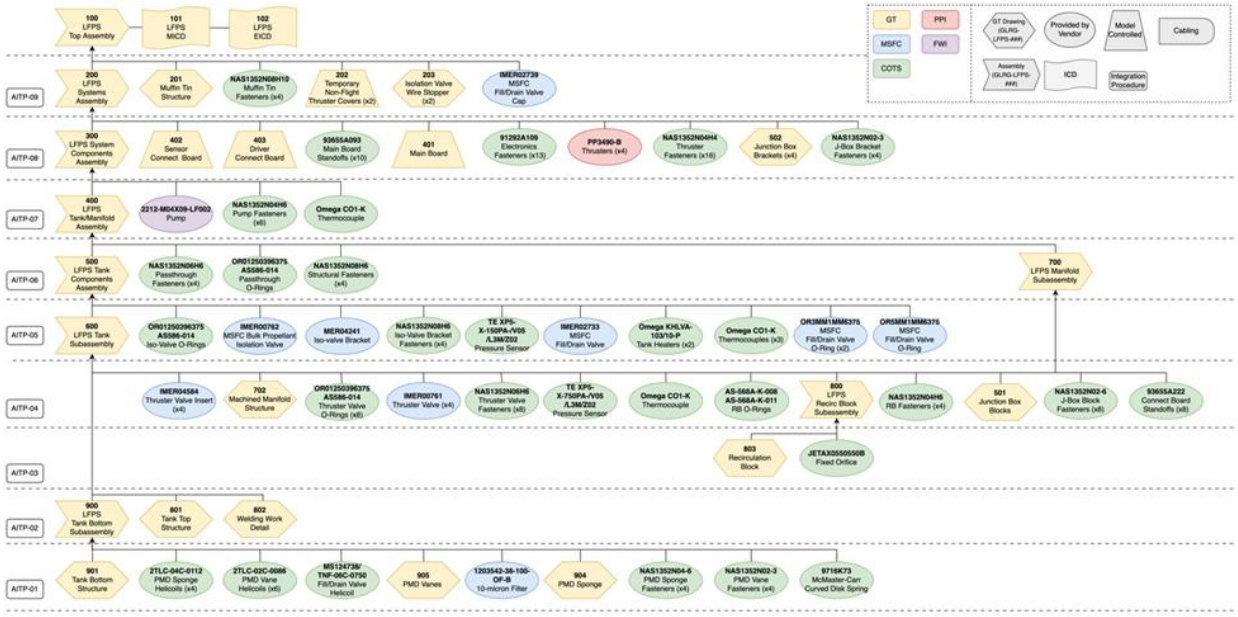

Figure 2: LFPS Product Breakdown Structure (PBS)

The steps to be performed within each AITP were detailed and controlled by an associated LFPS Assembly, Integration and Test (AI&T) Plan. Each AI&T Plan graphically detailed the assembly and test flow, and defined requirements for each AITP. An example is shown in Figure 3.

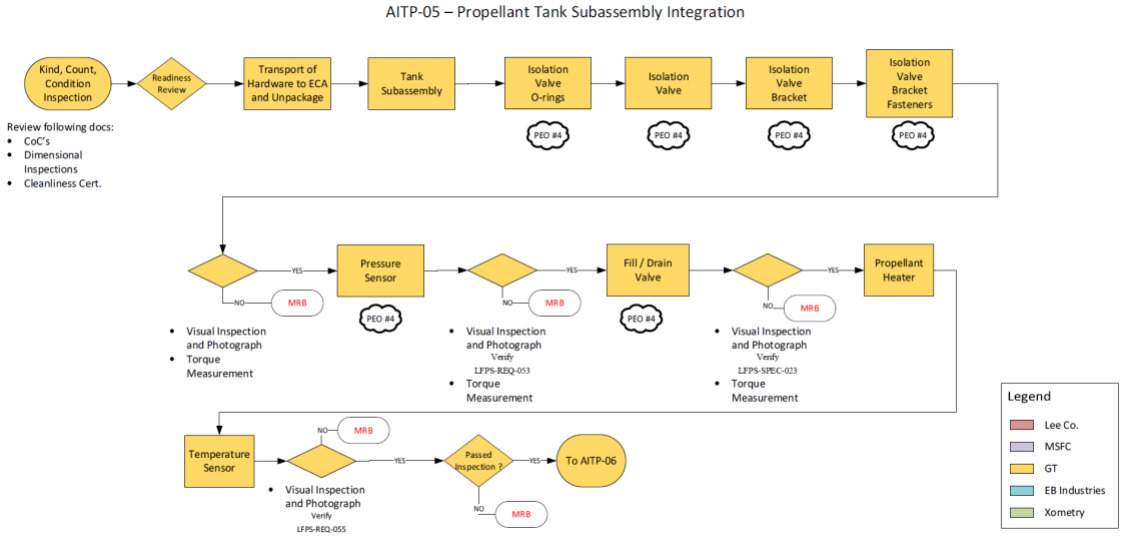

Figure 3: AITP-05 Propellant Tank Assembly Flow

As an example, AITP-05 – Propellant Tank Subassembly Integration governed the assembly, integration, and testing steps to build up that subassembly and included inspection points that required project sign-off to verify its proper completion – usually related to safety verifications. Details of the assembly process are shared in subsequent sections of this document.

Downloaded by GEORGIA INST OF TECHNOLOGY on February 26, 2022 | http://arc.aiaa.org | DOI: 10.2514/6.2022-1731

B. Wire Routing

Wire routing is often an afterthought, but the small size of CubeSats can make wire routing unforgiving. The MSFC and GT team was very intentional and forward thinking in wire management. For example, space between the top plate, “muffin tin” and tank was added to allow valve wires under the plate. Even then, the assembly was not without challenges, but they would have been far worse if wire routing was not considered early in the design.

A full-scale model of the LFPS was printed in plastic and assembled piece by piece just like the flight system. This gave the team an analog representation in which to work out the order of operations for assembly and consider features and layouts that were needed for wire routing. Practicing wire integration on the 3D printed unit revealed that the valve wires were stiffer than expected and would need a larger channel to keep them from extending outside of the enclosure limits set by the mechanical interface control document (ICD). A groove was cut into the 3D model to determine the best placement to make a modification, then the tanks were re-machined to incorporate the fix.

Wires were also laid out on the 3D model and measured so wires could be cut to the correct lengths and crimped prior to integration. One problem was that measurements were too conservative, so that after the initial measurement an additional 0.25” was added as margin; but on a CubeSat, this can be a significant length of wire. An example of the practice wiring vs real wiring is shown in Figure 4 . Note the x-pattern on the heater wires. Wiring diagrams were also created based on wiring on the 3D printed model and provided as a deliverable to the project.

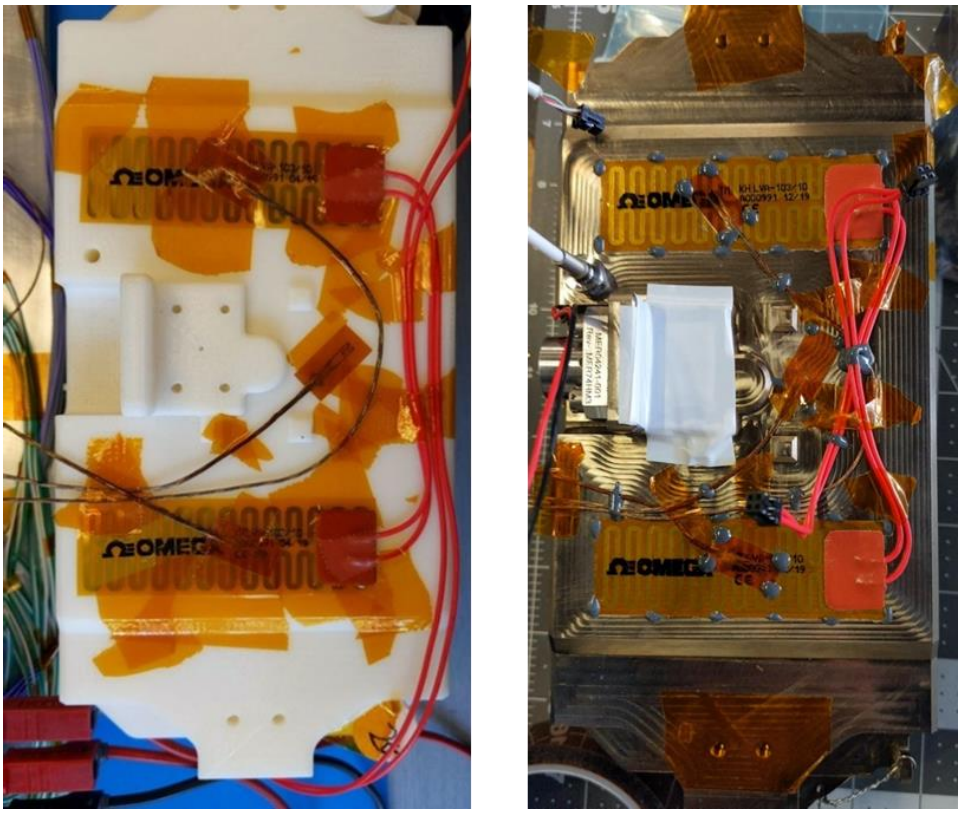

Figure 4. Tank Heater and Thermocouple Example Routing (left), and Flight Routing (right)

Downloaded by GEORGIA INST OF TECHNOLOGY on February 26, 2022 | http://arc.aiaa.org | DOI: 10.2514/6.2022-1731

C. Assembly Aids and Techniques

Numerous assembly techniques and aids were creatively used throughout the assembly process. Support at Georgia Tech allowed wide access to 3D printing capabilities. 3D printed fixtures, jigs, stands, and fixators were leveraged for every stage of assembly. Each stage of the assembly process had a custom 3D printed mounting fixture. This allowed for every subassembly to be fully secured but also be accessible for integration. The custom fixtures were designed to line up with the existing mounting holes on the tank bottom and manifold. They attached to a standardized base plate with aluminum 8020 rails and were swapped out to fit the appropriate subassembly.

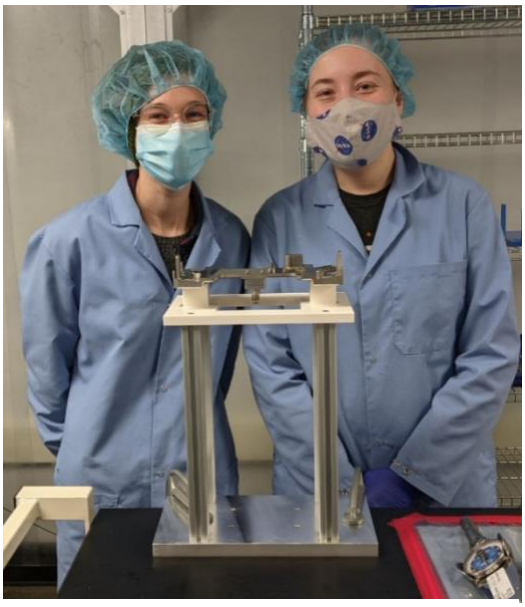

Figure 5: The Manifold on Assembly Fixture

During AITP-06, the tank and manifold had to be mounted very precisely to ensure alignment for the solar panel mounting holes. The tank and manifold were both attached to the solar panel deployment fixture with number 0 screws that needed to be placed in a vertical line within a +/- .01" tolerance. To accomplish this alignment, a custom fixture was 3D printed to hold several precision squares and offset screws that could press the faces of the manifold and tank into the appropriate positions before torquing down the two subassemblies.

Figure 6: The Tank Manifold Mounting Process with the GSE Fixture

Various 'fixators' were designed and printed to assist in the epoxy adhesion on surfaces mounted devices on various components such as the propellant tank, the pump, and a thruster valve. These fixators were design to mount to various sizes of commercial "quick grip" tools from hardware stores and were extremely helpful in the installation of heaters and thermocouples. The various fixators are shown in Figure 7.

Downloaded by GEORGIA INST OF TECHNOLOGY on February 26, 2022 | http://arc.aiaa.org | DOI: 10.2514/6.2022-1731

The round profiles of the valve and pump required specific fixators created that matched their radius of curvature to hold evenly distributed pressure onto the thermocouples while curing. The fixators for the large heaters included an additional EPDM pad to help better distribute the clamping forces on the heater and permit some conformance to small changes in adhesive thickness. The type of epoxy that was used will bond to the plastic fixators but does not bond to parchment paper. The fixtures were lined with parchment paper prior to use to ensure the plastic did not adhere to the hardware.

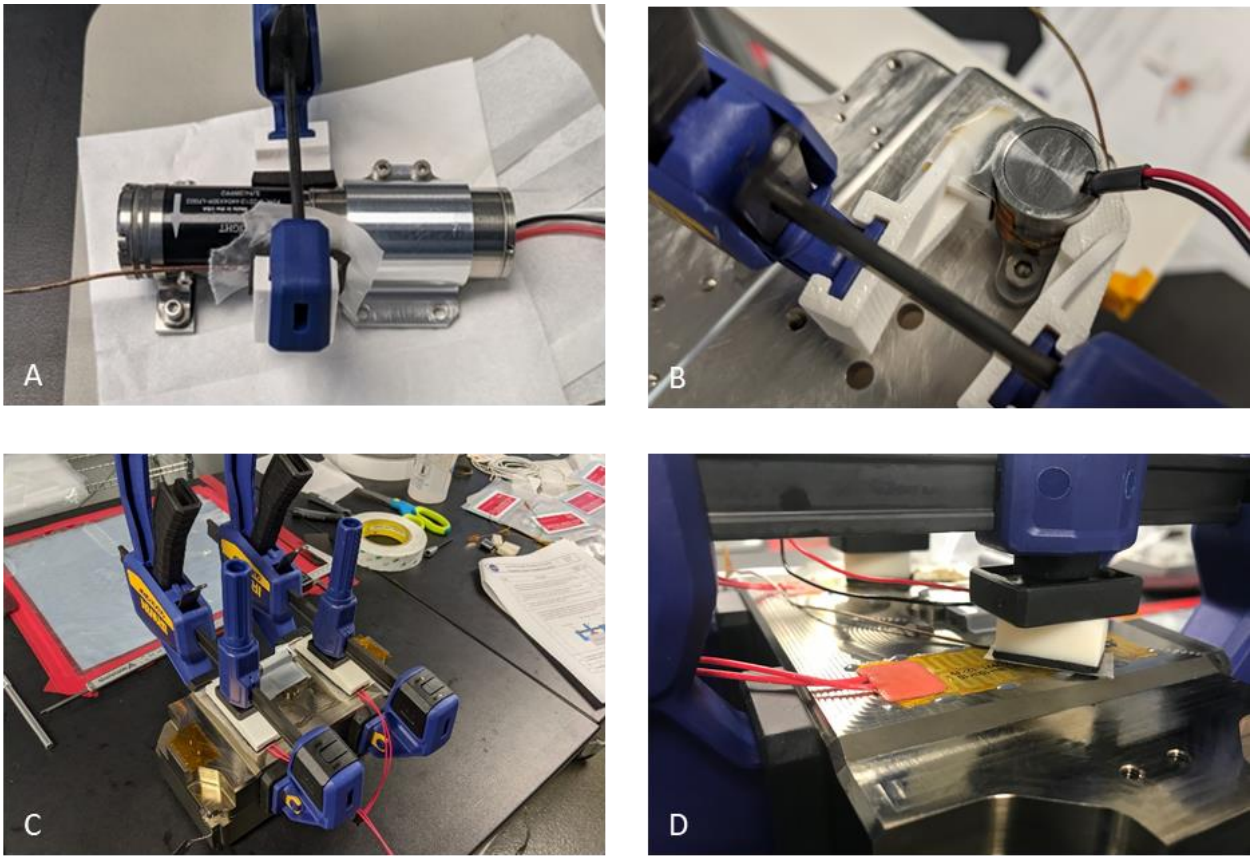

Figure 7: Various fixators used on LFPS. A) Pump thermocouple Fixator, B) Thruster Valve Thermocouple Fixator, C) Prop Tank Heater Fixators, and D) Prop Tank Heater Thermocouple Fixators

Downloaded by GEORGIA INST OF TECHNOLOGY on February 26, 2022 | http://arc.aiaa.org | DOI: 10.2514/6.2022-1731

The propellant tank required two thin Kapton tape heaters to warm up the fuel. The two heaters were applied by laying a thin strip of pressure sensitive adhesive (PSA) and clamping them to the surface of the tank as shown in Figure 7. The PSA required curing at elevated temperatures for several hours to property set. A low cost, custom curing oven was built from aluminum foil faces, foam board, a 150W incandescent lightbulb, a dimmer switch, and a wireless temperature sensor. Experimentation informed the dimmer switch – oven temperature correlation. To verify the heater-PSA-prop tank thermal bond, the heaters were turned on and heater was imaged with a FLIR thermal camera. The team had previously defined acceptance criteria for the allowable temperature variation across the heater. This process was developed in consultation with another MSFC spaceflight project. The heaters were then staked with epoxy to ensure that none of the edges would peel up.

Figure 8: Tank Heater Verification by FLIR

IV. System Level Verifications

After assembly of the LFPS was completed, system requirement validation and performance testing was conducted in the final AITPs.

A. System Leakage Rate Verification (Performed in AITP-08)

After integration, it was necessary to perform a flow rate and leakage rate test on each thruster. The flow test verified that all the internal passageways through the system were not clogged and that each thruster was passing its expected mass flow rate for the given input pressure. This test was accomplished by pressurizing the tank with a regulated helium supply, opening the isolation valve, opening the thruster valve, and measuring the gas flow rate through the thruster by a rotameter attached to its nozzle. The Project had previously determined gas flow rate acceptance criterion, informed by the thruster vendor's supplied data. This criterion was established for 100psia feed pressure; the tank maximum design pressure (MDP). All four thrusters had a flow rate which measured directly in the middle of their acceptable range. Therefore, they all passed without issues.

Then, with the tank pressurized with helium to MDP, all the valves were closed, and the system was placed into a vacuum chamber connected to a helium mass spectrometer. The vacuum chamber was depressurized, and the mass spectrometer attempted to detect any helium that could be leaking from the system. So little was detected that the reported leakage was lower than the control measurement taken without the tank being inside. These two tests verified that the system leakage rate was far below the specified allowable.

Downloaded by GEORGIA INST OF TECHNOLOGY on February 26, 2022 | http://arc.aiaa.org | DOI: 10.2514/6.2022-1731

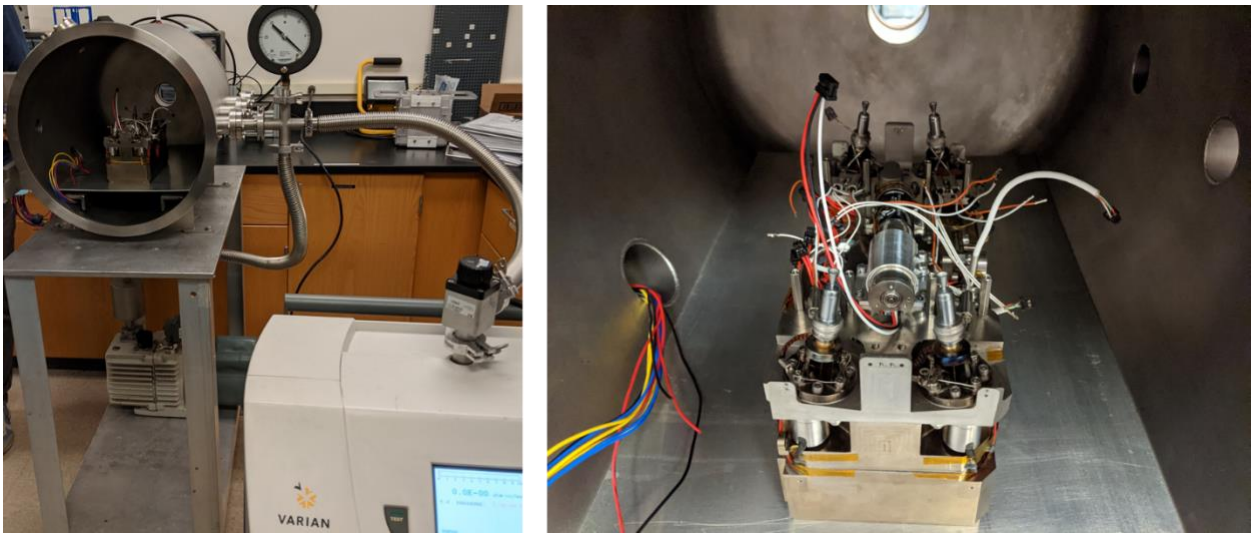

Figure 9: LFPS Undergoing Vacuum Bell Jar Leak Testing

B. Mass and Dimensional Verifications (Part of AITP-09)

Dimensional and mass measurements were taken to verify the final hardware complied with the ICD specifications. Component and subassembly level masses were recorded throughout the assembly process and integrated into the Master Equipment List (MEL).

The structural dry mass of the propulsion system is very important, because the total spacecraft mass is limited by the launch vehicle, and the dry mass influences the amount of propellant that can be loaded on the spacecraft. During the design phase, an expected mass list was created that detailed the anticipated mass of each individual component. The project followed the AIAA S-120 ‘Mass Properties Control for Space Systems’ and applied appropriate mass growth allowances (MGAs) to each part dependent on their maturity level. However, the Project observed that the MGAs were found to be conservative when used on the small spacecraft scale. The completed LFPS weight very close to its baseline mass without MGAs. It could be argued that the AIAA S-120 MGAs do not translate well to the CubeSat scale, and that future project may reassess their application.

C. System Power Verification (Performed in AITP-09)

After assembly of the LFPS was completed, the Powered Equipment List (PEL) was verified by performing system-level electrical liveliness tests and ‘day in the life’ thermal vacuum (TVAC) testing. A benchtop power supply was used for accurate power draw data. Each powered device was cycled on, and the power draw recorded. This data was used to validate the calculated PEL values and verify the power per mode specification. This test series was also used to develop and demonstrate firmware functionality and recommended command sequencing and timing to reduce power consumption while initializing the LFPS and pre-heating the thrusters. Furthermore, this test provided verification of the thermal model of LFPS and informed the expected heat generated during each stage of operation.

Downloaded by GEORGIA INST OF TECHNOLOGY on February 26, 2022 | http://arc.aiaa.org | DOI: 10.2514/6.2022-1731

During system level acceptance testing of the LFPS extensive thruster pre-heat testing was performed. It was a requirement that the thrusters achieve pre-heat temperature while using less than 47 W power. As part of the system power verification, the unit was taken down to vacuum and the thrusters completed their warmup sequence using a firmware-driven 'derating' mode to keep the instantaneous power draw below 47 W. Figure 10 shows the thermocouples on the thruster tracking with K-type thermocouples that were placed slightly upstream from the R-type thruster thermocouples. The power drawn scale is shown on the right axis.

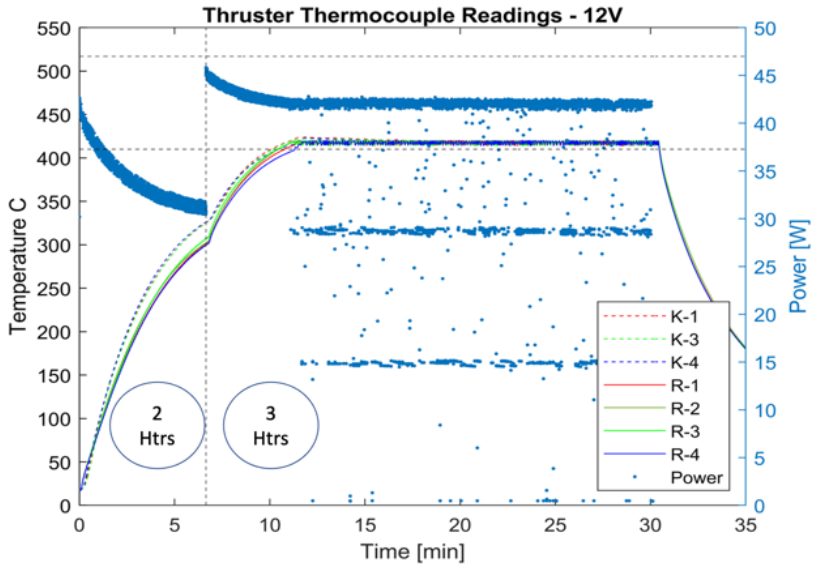

Figure 10. Thruster Warm Up Curves

The LFPS thrusters underwent acceptance testing prior to delivery to the project. During this testing it was discovered that in the junction boxes, T-type thermocouple extension wire was used rather than R-type as expected. Remarkably, this was an issue that began at the wire manufacturer. The wire was incorrectly identified, and color coded as Type R extension wire. The splice between the erroneous thermocouple wire and the thermocouple behaves like another thermocouple and distorts the intended measurement. The LFPS Project assessed options to use as is and elected to move forward with an operational fix to compensate for the error.

During the power testing, thin K-type thermocouples were inserted into the catalyst bed as shown in Figure 11. This test showed that the "R-type" and K-type thermocouples read very close to each other and were accurate at the expected preheat temperatures as shown in Figure 10. Due to their placement positions the K-type thermocouples were expected to be about 10 °C higher than the R-type. A possible explanation was that the junction boxes were very close in temperature to the thermocouple amplifiers on the controller board, which have cold junction compensation. Thus, they were able to compensate for the extra junction and provide accurate temperature measurements.

Downloaded by GEORGIA INST OF TECHNOLOGY on February 26, 2022 | http://arc.aiaa.org | DOI: 10.2514/6.2022-1731

Downloaded by GEORGIA INST OF TECHNOLOGY on February 26, 2022 | http://arc.aiaa.org | DOI: 10.2514/6.2022-1731

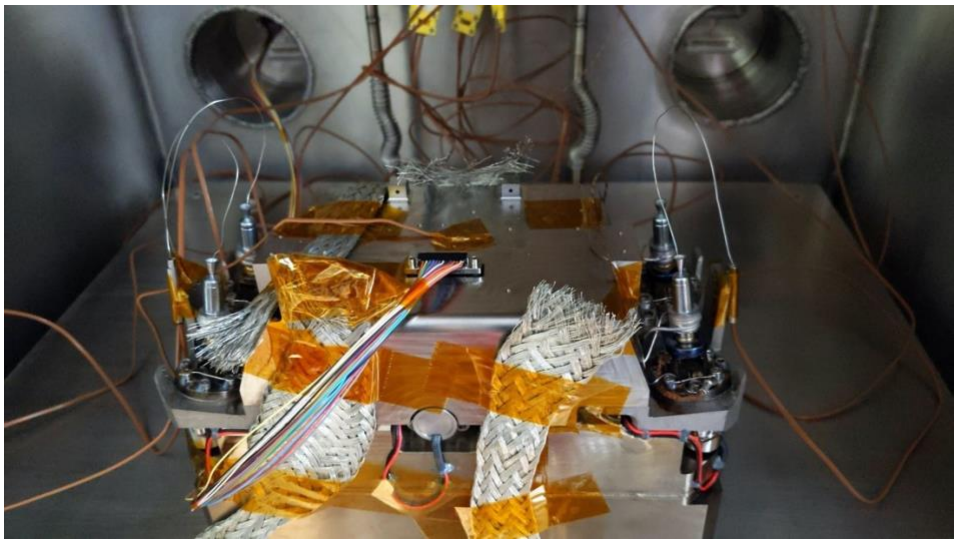

Figure 11. LFPS Thrusters with Thermocouples

V. Protoflight Qualification

The flight unit used a hybrid qualification – protoflight acceptance approach. Because there was not going to be a protoflight acceptance test program, the project added qualification and acceptance test requirements for the components and major subassemblies of the LFPS. This approach is summarized in Figure 12. Each major component (pump, thrusters, valves, and controller) had its own qualification campaign to demonstrate the design and manufacturing processes were suitable to meet the mission's requirements. Additionally, each component has its own acceptance test campaign prior to integration into the flight system.

	Testing Campaigns	Flight Qualification					Flight Acceptance				
		Radiation Testing	Random Vibration	Thermal Vacuum	Performance Life	Proof & Burst	Random Vibration	Thermal Vacuum	Proof & Leak	Hot Fire	End – End Functional
Components	100mN Thrusters	--	Qual Levels & Durations	--	Per Test Plan	--	Acceptance Levels & Durations	--	MDP X 1.5	Per Test Plan	FlatSat
	Pump	--	Qual Levels & Durations	Qual Margins (4 Cycles)	Per Test Plan	MDP X 2.5	Acceptance Levels & Durations	Acceptance Margins (4 Cycles)	MDP X 1.5	--	FlatSat
	Solenoid Valve	--	Qual Levels & Durations	Qual Margins (4 Cycles)	Per Test Plan	MDP X 2.5	Acceptance Levels & Durations	Acceptance Margins (4 Cycles)	MDP X 1.5	--	FlatSat
	Fill/Drain Valve	--	Qual Levels & Durations	Qual Margins (4 Cycles)	Per Test Plan	MDP X 2.5	Acceptance Levels & Durations	Acceptance Margins (4 Cycles)	MDP X 1.5	--	--
	Controller	TID & SEE (Prototype)	Qual Levels & Durations	Qual Margins (4 Cycles)	Per Test Plan	--	Acceptance Levels & Durations	Acceptance Margins (2 Cycles)	--	--	--
	Propellant Tank	--	--	--	Per Test Plan	MDP X 2.5	--	--	MDP X 1.5	--	--
	Manifold	--	--	--	--	MDP X 2.5	--	--	MDP X 1.5	--	--
	LFPS System	--	--	--	--	--	SC Protoflight Levels & Durations	SC Protoflight Levels & Durations	MDP X 1.1	--	AITP-09

Vendor
MSFC
GT
JPL

Figure 12: LFPS Hybrid Qualification Approach

As an example, acceptance testing was conducted on the flight controller boards by Georgia Tech prior to integration. Thruster acceptance testing and qualification was performed by the vendor, Plasma Processes LLC (Huntsville, AL). Valve acceptance and qualification was performed by MSFC.

VI. Controller

The LFPS includes three printed circuit boards (PCBs) that implement control loops, accept commands, and send telemetry. The microcontroller utilizes FPrime, an open-source flight software framework made available by JPL. The flight controller boards were printed in December 2020, underwent environmental flight acceptance testing in February 2021, and were integrated into the system in April 2021.

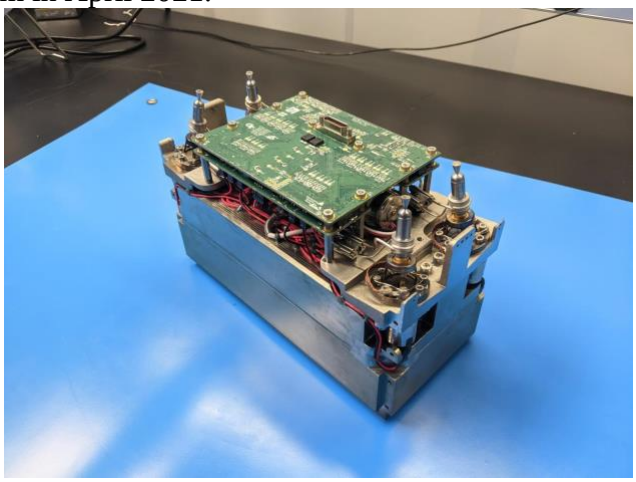

Figure 13. Controller Mounted on LFPS

A. Random Vibration Acceptance Testing

This test consisted of applying random vibration loads to each axis of the controller, to ensure survival due to vibration loads inherent to the launch vehicle. The controller boards were stacked onto an aluminum plate test fixture using the same procedure that would be followed when installing onto the manifold during final flight integration. This included applying adhesive to the threading and torquing to the expected values. The test began with a full functional test which included use of each driver and sensor channel as well as current/voltage readings to ensure nominal performance.

Downloaded by GEORGIA INST OF TECHNOLOGY on February 26, 2022 | http://arc.aiaa.org | DOI: 10.2514/6.2022-1731

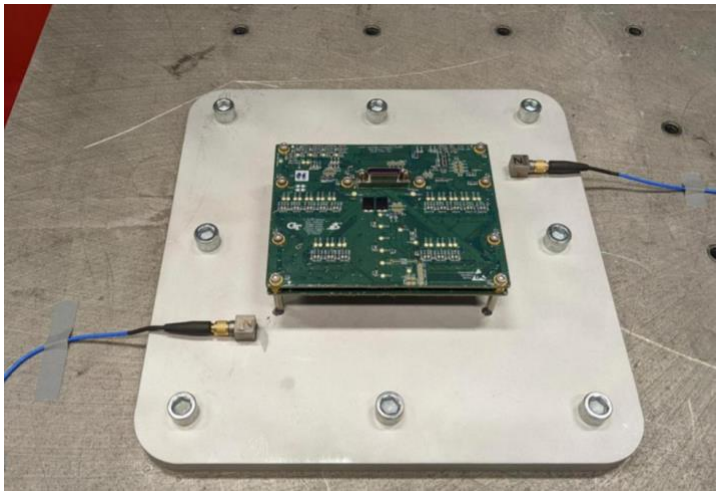

Figure 14. Flight hardware on fixture

Next, the flight controller underwent random vibration tests of each axis at acceptance levels for 60 seconds per axis. Between each axis a simple functional test was run and after the acceptance test a full functional test was run. The simple functional test exercised the driver and sensor channels farthest from supports to ensure functionality remained throughout the test. This would help to narrow down the timeframe where damage to the controller would have occurred. However, no degradation in performance was seen during these tests.

Figure 15. Short functional test during flight acceptance random vibe testing

B. Thermal Vacuum Acceptance Testing

Following successful random vibration testing, acceptance level thermal vacuum testing was performed. This test consisted of cycling the controller between maximum and minimum temperature setpoints to verify that the device continues to operate after thermal stress.

As seen in Figure 16, the test was performed by alternating the temperature of the controller between maximum and minimum setpoints. The chamber was brought under 0.75 torr before

Downloaded by GEORGIA INST OF TECHNOLOGY on February 26, 2022 | http://arc.aiaa.org | DOI: 10.2514/6.2022-1731

commencing the thermal cycling. The controller was then cycled between the minimum and maximum operational temperatures for 1 hour each, with a functional test at the end of each dwell time. During the last 2 operational extreme tests, a thermal control loop test was performed after the normal functional test to verify that the controller could thermostatically control its temperature using its onboard heater. Finally, the chamber was brought back to ambient pressure and the chamber was flushed with air. To close out the test procedure, a final full functional test was performed. The flight boards successfully passed each of these checks and thus passed the environmental testing requirement for the Lunar Flashlight mission.

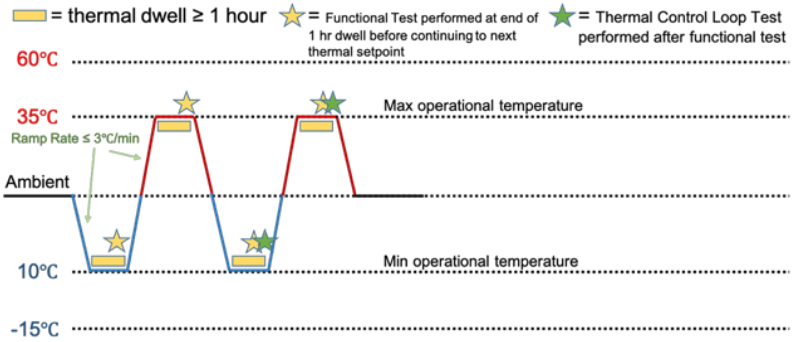

Figure 16. Thermal Cycling Chart

The thermal vacuum test was performed in a chamber which has a temperature range of -20 °C to 60 °C. Due to the large mass of the controller test stand and thermal radiation from the chamber walls, precautions had to be implemented to reach the required cold temperature of 10 °C on the controller board. This included the use of copper thermal straps, thermal grease between the test fixture and chamber platen, and aluminum foil around the test article to block radiative heat from the chamber walls. The final test configurations are shown in Figure 17.

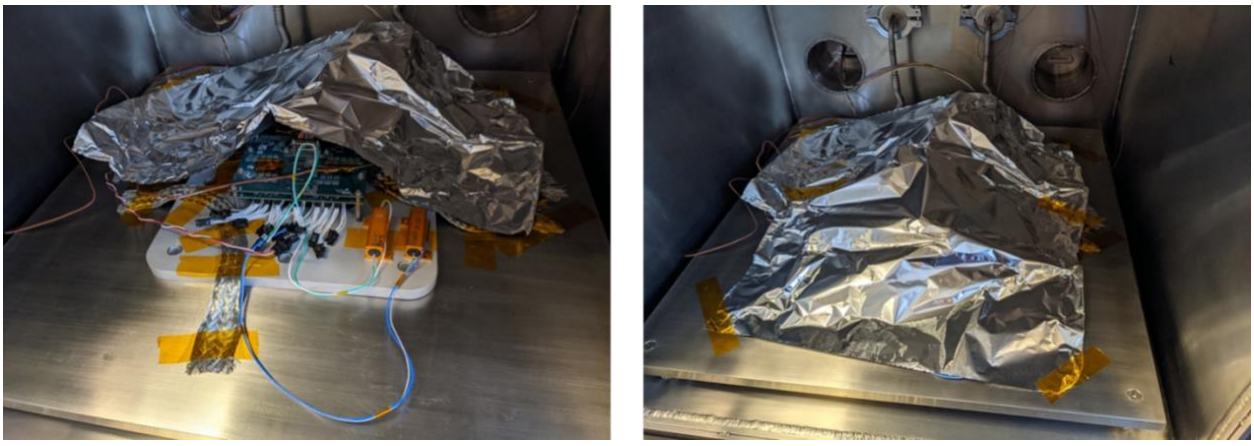

Figure 17. Flight controller with thermal straps and aluminum foil (left), and Flight controller completely covered with aluminum foil (right)

Downloaded by GEORGIA INST OF TECHNOLOGY on February 26, 2022 | http://arc.aiaa.org | DOI: 10.2514/6.2022-1731

C. Firmware and Parameter Testing

Simultaneous with environmental test, the LFPS flight firmware was also finished and tested. An electronics Flat-Sat was fabricated that mimicked each component of the flight system allowing a full test of the inputs and outputs of the controller. Relays were used in place of thruster and ISO valves, chassis mounted resistors emulated heaters, and a motor emulated the pump. Adjustable Wheatstone bridges emulated the pressure sensors and thermocouples [2].

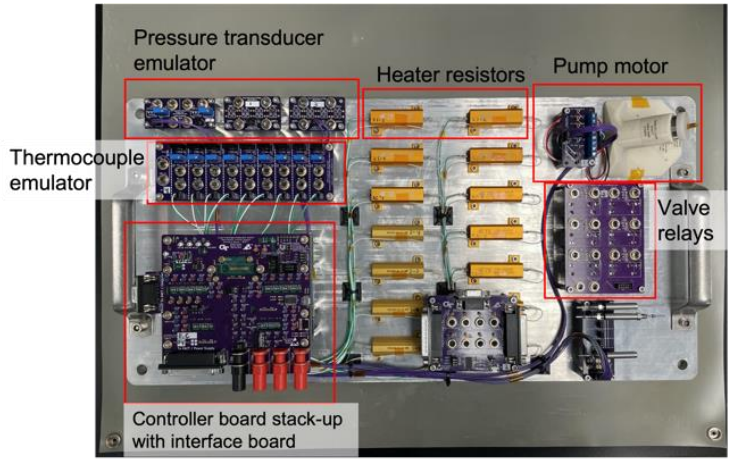

Figure 18. The LFPS electronics Flat-Sat

The first phase of firmware testing occurred on the Flat-Sat with a Python scripted test that could run for many hours. The Flat-Sat was set to a known state, with thermocouple and pressure sensors at pre-set temperature and pressure emulated values. First, the script ran the concept of operations, turning on the tank heaters, opening the ISO valve, running the pump, and sending random thrust commands for an extended period. Throughout this operation, the script verified information in telemetry such as command count, valve/heater state, valve/heater current readings, status flags, etc.

Next, an operator test occurred using the graphical user interface (GUI) build for the LFPS as shown in Figure 19. State based faults were exercised, for example, opening the isolation valve, running the pump, and having a thruster catalyst heater too cold to fire successfully. The heater derate modes were tested and visually confirmed. The operator then ran through a more robust version of the propulsion system concept of operations and the state machine transitions were exercised for each component.

Downloaded by GEORGIA INST OF TECHNOLOGY on February 26, 2022 | http://arc.aiaa.org | DOI: 10.2514/6.2022-1731

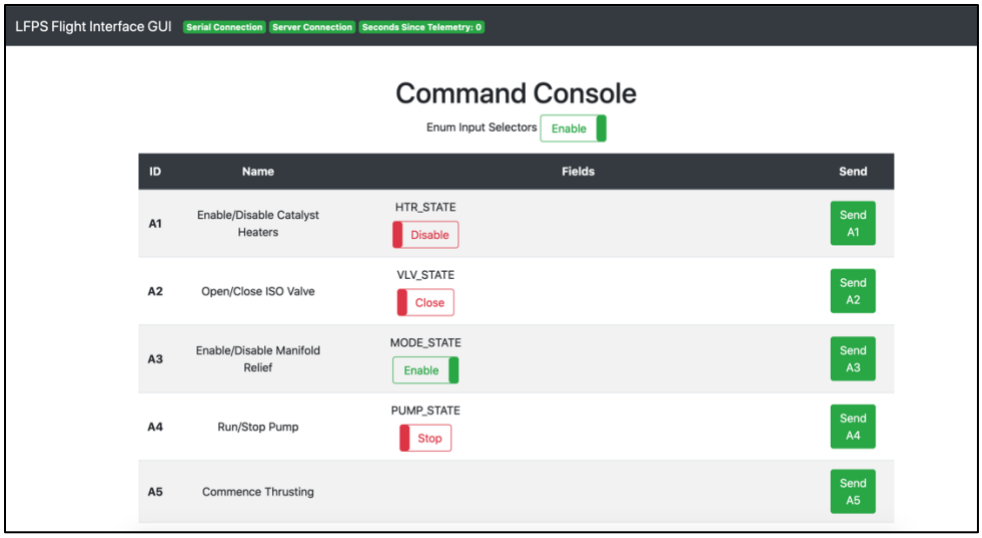

Figure 19. LFPS Direct Exerciser GUI

Further firmware testing occurred at JPL on a version of the GT Flat-Sat that was connected to the Lunar Flashlight flight software system.

VII. Full Flat-Sat Testing at MSFC

An acceptance requirement and planned action following delivery to JPL was to conduct the concept of operations on a mechanical Flat-Sat. This test was performed at MSFC in August 2021. The test utilized flight spares of a pump, ISO valve, and thruster as well as an engineering unit LFPS controller board.

During this test, it was discovered that the current configuration of the pump motor control loop parameters could not properly manage the added load of the propellent. The motor controller used a proportional-integrator (PI) gain controller. Table 1 summarizes the changes in steady state and transient gain value changes. The increase in the speed control acceleration limit allowed the motor to reach the desired speed faster.

Table 1. Pump Motor Parameter Changes

Parameter Name	Abbreviation	Old Value	New Value
Steady-State Commutation Controller Proportional Gain	CP	10	9 ↓
Steady-State Commutation Controller Integral Gain	CI	3	7 ↑
Transient Commutation Controller Proportional Gain	CPT	5	9 ↑
Transient Commutation Controller Integral Gain	CIT	3	7 ↑
Speed Control Acceleration Limit	SGL	9	12 ↑

Downloaded by GEORGIA INST OF TECHNOLOGY on February 26, 2022 | http://arc.aiaa.org | DOI: 10.2514/6.2022-1731

After gain values were tuned, hot fire testing was successfully performed on the LFPS Flat-Sat configuration.

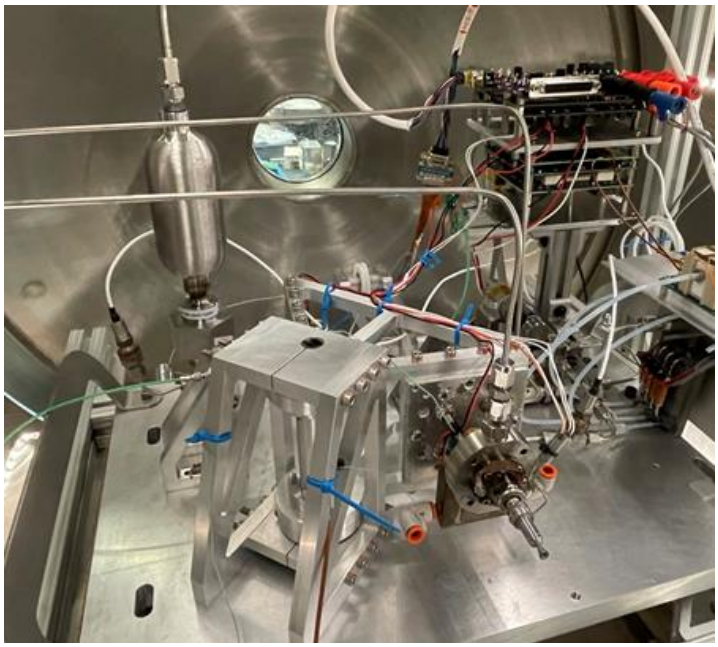

Figure 20. Mechanical Flat-Sat at MSFC

VIII. Continuing Work

LFPS was integrated into the LF spacecraft in fall 2021. Continuing support has been provided for testing the propulsion system during spacecraft integration and testing. Additionally, the system will be fueled at MSFC prior to delivery to the launch vehicle at Cape Canaveral. Fueling is Planned for January 2022.

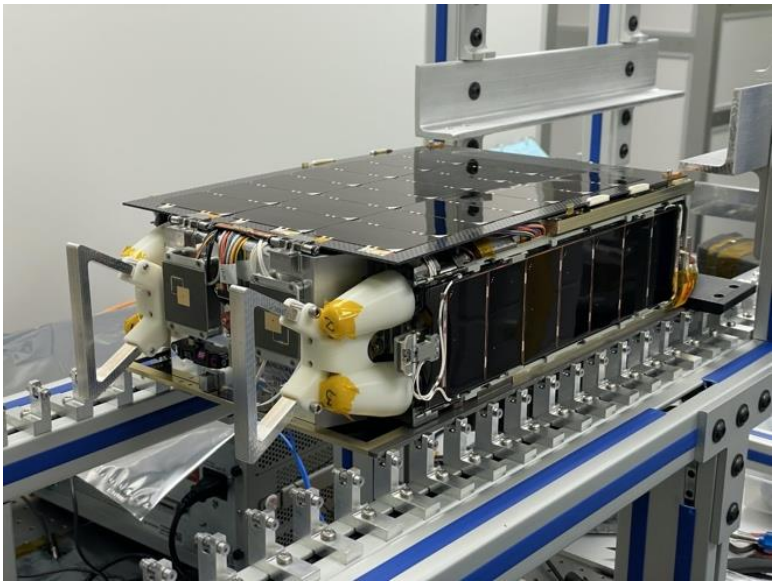

Figure 21. LFPS Integrated into Lunar Flashlight

Downloaded by GEORGIA INST OF TECHNOLOGY on February 26, 2022 | http://arc.aiaa.org | DOI: 10.2514/6.2022-1731

A second LFPS unit is currently being integrated with the spare parts of the assembly of LFPS as a low-cost propulsion system for a future mission. Additionally, with the heritage from the LFPS, more propulsion systems like this one are being developed due to its small form factor, safe fuel, and relatively high thrust capability.

Acknowledgments

The authors wish to acknowledge those who supported the Lunar Flashlight Propulsion System team at the NASA Marshall Spaceflight Center, the Jet Propulsion Laboratory, and Georgia Tech for their continuing technical and managerial support to the project.

- Georgia Tech Contributors: Grayson Huggins, Ali Talaksi, Nathan Cheek, Nathan Daniel, Brandon Cólon, and Mackenzie Glaser
- MSFC Contributors: Carlos Diaz, McKynzie Perry, Chris Burnside
- JPL Contributors: John Baker, Matt Kowalkowski, Frank Picha

The authors would also like to acknowledge the NASA Grant (80NSSC20K1476) and NASA Cooperative Agreement (80MSFC19M0044) that funded this phase of work on the Lunar Flashlight Propulsion System at the Georgia Tech Space Systems Design Laboratory.

Downloaded by GEORGIA INST OF TECHNOLOGY on February 26, 2022 | http://arc.aiaa.org | DOI: 10.2514/6.2022-1731

References

[1] Andrews, D., Lightsey, E.G.; "Design of a Green Monopropellant Propulsion System for the Lunar Flashlight Mission," Masters Report, Georgia Institute of Technology, December 2019.

[2] Cheek, N., Daniel, N., Lightsey, E.G., Peet, S., Smith, C., Cavender, D.; "Development of a COTS-Based Propulsion System Controller for NASA's Lunar Flashlight CubeSat Mission", SSC21-IX-06, AIAA 35th Annual Small Satellite Conference, August 2021.

[3] Huggins, G.M., Talaksi, A., Andrews, D., Lightsey, E.G., Cavender, D., McQueen, D., Williams, H., Diaz, C., Baker, J., Kowalkowski, M.; "Development of a CubeSat-Scale Green Monopropellant Propulsion System for NASA's Lunar Flashlight Mission," AIAA 2021-1976, AIAA SciTech 2021 Forum, January 2021.

[4] Huggins, G., Lightsey, E.G.; "Development of a CubeSat-Scale Green Monopropellant Propulsion System for NASA's Lunar Flashlight Mission", Masters Report, Georgia Institute of Technology, August 2020.

[5] Talaksi, A., Lightsey, E.G.; "Manufacturing, Integration, and Testing of the Green Monopropellant Propulsion System for NASA's Lunar Flashlight Mission," Masters Report, Georgia Institute of Technology, December 2020.

[6] Cohen, B. A., Hayne, P. O., Greenhagen, B., Paige, D. A., Seybold, C., and Baker, J., "Lunar Flashlight: Illuminating the Lunar South Pole," IEEE Aerospace and Electronic Systems Magazine, Vol. 35, No. 3, Mar. 2020, pp. 46–52.

Downloaded by GEORGIA INST OF TECHNOLOGY on February 26, 2022 | http://arc.aiaa.org | DOI: 10.2514/6.2022-1731